



BGK electron solitary waves: 1D and 3D

L.-J. Chen, G. K. Parks

► To cite this version:

L.-J. Chen, G. K. Parks. BGK electron solitary waves: 1D and 3D. *Nonlinear Processes in Geophysics*, 2002, 9 (2), pp.111-119. hal-00302084

HAL Id: hal-00302084

<https://hal.science/hal-00302084>

Submitted on 1 Jan 2002

HAL is a multi-disciplinary open access archive for the deposit and dissemination of scientific research documents, whether they are published or not. The documents may come from teaching and research institutions in France or abroad, or from public or private research centers.

L'archive ouverte pluridisciplinaire **HAL**, est destinée au dépôt et à la diffusion de documents scientifiques de niveau recherche, publiés ou non, émanant des établissements d'enseignement et de recherche français ou étrangers, des laboratoires publics ou privés.

BGK electron solitary waves: 1D and 3D

L.-J. Chen¹ and G. K. Parks²

¹Physics Department, University of Washington, Seattle, WA, 98195, USA

²Space Science Laboratory, University of California, Berkeley, CA, 94720, USA

Received: 27 October 2001 – Accepted: 3 December 2001

Abstract. This paper presents new results for 1D BGK electron solitary wave (phase-space electron hole) solutions and, based on the new results, extends the solutions to include the 3D electrical interaction ($E \sim 1/r^2$) of charged particles. Our approach for extending to 3D is to solve the nonlinear 3D Poisson and 1D Vlasov equations based on a key feature of 1D electron hole (EH) solutions; the positive core of an EH is screened by electrons trapped inside the potential energy trough. This feature has not been considered in previous studies. We illustrate this key feature using an analytical model and argue that the feature is independent of any specific model. We then construct azimuthally symmetric EH solutions under conditions where electrons are highly field-aligned and ions form a uniform background along the magnetic field. Our results indicate that, for a single humped electric potential, the parallel cut of the perpendicular component of the electric field (E_{\perp}) is unipolar and that of the parallel component (E_{\parallel}) bipolar, reproducing the multi-dimensional features of the solitary waves observed by the FAST satellite. Our analytical solutions presented in this article capture the 3D electric interaction and the observed features of E_{\parallel} and E_{\perp} . The solutions predict a dependence of the parallel width-amplitude relation on the perpendicular size of EHs. This dependence can be used in conjunction with experimental data to yield an estimate of the typical perpendicular size of observed EHs; this provides important information on the perpendicular span of the source region as well as on how much electrostatic energy is transported by the solitary waves.

1 Introduction

Solitary waves are coherent wave structures arising from the balance of nonlinearity and the dispersive effect of a medium (Drazin, 1984, and references therein). They have been recognized to be an ideal way of transporting energy, charge or

information (Davydov, 1985; Hasegawa and Kodama, 1995) owing to the fact that they retain their shape and velocity during propagation. In the last two decades, solitary potential structures have been observed in many dynamical regions of the Earth's magnetosphere: the plasma sheet boundary (Matsumoto et al., 1994; Cattell et al., 1999; Franz et al., 1998), auroral ionosphere (Temerin et al., 1982; Boström et al., 1988; Mälkki et al., 1993; Eriksson et al., 1997; Mozer et al., 1997; Ergun et al., 1998a, 1998b, 1999), bow shock (Bale et al., 1998; Matsumoto et al., 1998) and magnetosheath (Kojima et al., 1997). The question of what role(s) these solitary waves play in the dynamics of space plasma has been of great interest to researchers and still requires a substantial amount of observational and theoretical effort.

Solitary waves with either positive or negative potentials have been observed. Negative potential pulses observed in the auroral upward current region (Boström et al., 1988; Mälkki et al., 1993) have been shown to possess properties that are consistent with Bernstein-Greene-Kruskal (BGK) ion mode solitary waves in 1D (Bernstein et al., 1957; Mälkki et al., 1989). Positive potential pulses detected in the auroral downward current region (Ergun et al., 1998a, 1998b, 1999) show features that are consistent with BGK electron mode solitary waves (Muschiatti et al., 1999), also called phase space electron holes (Turikov, 1984). These solitary waves have velocities parallel to the geomagnetic field and directed out of the ionosphere (Boström et al., 1988; Eriksson et al., 1997; Ergun et al., 1998a, 1998b, 1999). Since solitary wave potentials trap charged particles, the outward propagating solitary waves offer a means for transporting electrostatic energy and charge into the magnetosphere. However, it is not yet known how significant this transport mechanism is. Encouraged by the good agreement between 1D BGK models and the parallel behavior of solitary waves (Mälkki et al., 1989; Muschiatti et al., 1999), we analytically construct 3D BGK solutions to model the positive potential pulses observed by the FAST satellite (Ergun et al., 1998a, 1998b, 1999), with the objective of obtaining further information on the roles played by solitary waves in ionospheric and magne-

tospheric dynamics.

Positive potential pulses detected by the FAST satellite are multi-dimensional with bipolar E_{\parallel} and unipolar E_{\perp} (Ergun et al., 1998a, 1998b, 1999). Nonzero E_{\perp} indicates that the perpendicular span of the solitary structure is finite. This combined with the fact that the solitary waves are observed in a 3D environment dictates that a 3D model be constructed. The nature of electric interaction in 3D is different from that in 1D and 2D. The electric field of a charged particle in 3D is $E \sim 1/r^2$, where r is the distance from the particle. In 1D, E is constant over distance and the 3D equivalence of this constant field is produced by an infinite charge sheet. In 2D, $E \sim 1/r$ and the 3D equivalence of this field can be realized by an infinitely long line of charges. When solving a Poisson equation in less than 3D to explain physical features observed in a 3D world, one must address how these 3D equivalent systems are produced and whether their use to explain physical features is justified.

Electrons associated with solitary waves are highly field-aligned with a gyroradius ≤ 1 m, while the typical scale size of the solitary waves and the Debye length λ_D are ~ 100 m (Ergun et al., 1999). In this case, as a reasonably good approximation, the electrons can be treated as if they are confined to move only along the magnetic field. Thus, the Vlasov equation for electrons can be reduced to 1D (the dimension parallel to the magnetic field).

The role of electrons trapped in the solitary potential takes on fundamental importance in BGK solitary waves (Bernstein et al., 1957). In Sect. 2, we will deduce the feature of screening-by-trapped-electrons, for 1D BGK phase space electron holes (EH), by analytically calculating the separate contributions from the trapped and passing electrons to the charge density. This feature will be used in Sect. 3, where we obtain azimuthally symmetric EH solutions to the coupled 3D Poisson and 1D Vlasov equations. We discuss the properties of these solutions and how they can enhance our understanding of the solitary waves observed in space.

2 Screening by trapped electrons

1D BGK EH solutions have been studied extensively since 1957, when BGK obtained the general solutions to the nonlinear time-independent Vlasov-Poisson equations. Discussions on general aspects of EHs, such as phase space orbits of electrons in the vicinity of a positive potential, can be found in textbooks (Krall and Trivelpiece, 1973; Davidson, 1972) as well as in research papers (Bohm and Gross, 1949; Goldman et al., 1999). The basic idea is to separate electrons into two populations: electrons that are trapped inside the potential pulse and those that are not (called passing electrons). As demonstrated by BGK (1957), trapped electrons are the source of nonlinearity and they play a crucial role in solitary wave solutions. However, the specific details as to how trapped and passing electrons contribute to macroscopic variables such as the charge density have not been addressed. EHs were taken to be positively charged (Roberts and Berk,

1967; Berk et al., 1970; Schamel, 1986; Krasovsky et al., 1999) and shielded by the ambient plasma (Schamel, 1986; Krasovsky et al., 1999). In this section, a completely different picture will be presented.

The charge density distribution for an EH can be computed from the second derivative of the potential. For a bell-shaped positive potential pulse, the charge density is negative at the flank and positive at the core (see, for example, Fig. 1b). We use the approach formulated by BGK to calculate the densities of trapped and passing electrons and demonstrate that the negative charge density at the flank comes exclusively from trapped electrons. In other words, the positive core is shielded by trapped electrons and not by the ambient electrons.

The time-independent, coupled Vlasov and Poisson equations, with the assumption of a uniform neutralizing ion background, take the following form:

$$v \frac{\partial f(v, x)}{\partial x} + \frac{1}{2} \frac{\partial \phi}{\partial x} \frac{\partial f(v, x)}{\partial v} = 0, \quad (1)$$

$$\frac{\partial^2 \phi}{\partial x^2} = \int_{-\infty}^{\infty} f(v, x) dv - 1, \quad (2)$$

where f is the electron distribution function and the quantities have been normalized with the units of the Debye length λ_D , the ambient electron thermal energy T_e and the electron thermal velocity $v_t = \sqrt{2T_e/m}$. The total energy $w = v^2 - \phi$ with this convention.

For demonstration, we use a Gaussian solitary potential,

$$\phi(\psi, \delta, x) = \psi e^{-x^2/2\delta^2}, \quad (3)$$

and Maxwellian passing electrons whose density has been normalized to 1 (the background ion density) outside the solitary potential,

$$f_p(w) = \frac{2}{\sqrt{\pi}} e^{-w}. \quad (4)$$

This case has been treated by Turikov (1984) to obtain the trapped electron distribution and to derive the width-amplitude relation for EHs with zero phase-space density at the hole center. We use the same starting point to calculate the number densities of trapped and passing electrons to illustrate their perspective role in how shielding is achieved.

Following the BGK approach, we obtain the expression for the trapped electron distribution as,

$$f_{tr}(\psi, \delta, w) = \frac{4\sqrt{-w}}{\pi\delta^2} \left[1 - 2 \ln \left(\frac{-4w}{\psi} \right) \right] + \frac{2e^{-w}}{\sqrt{\pi}} [1 - \text{erf}(\sqrt{-w})]. \quad (5)$$

The first term in f_{tr} stems from the potential and has a single peak at $w = \frac{-\psi}{4e^{3/2}}$. This term is 0 at $w = 0^-$, goes negative at $w = -\psi$ and will always be single peaked even for other bell-shaped solitary potentials (for example, $\text{sech}^2(x/\delta)$ and $\text{sech}^4(x/\delta)$, see Fig. 4 of the paper by Turikov (1984) for the

special case of empty-centered EHs). Although the peak location may vary, it will not be at the end points, 0 and $-\psi$. The second term arising from the integral of the passing electron distribution decreases monotonically from $w = 0^-$ to $w = -\psi$. The end point behavior of the two terms implies that $f_{tr}(w = 0^-) > f_{tr}(w = -\psi)$. Combining the behavior of the two terms in f_{tr} , it can be concluded that $f_{tr}(0 > w \geq -\psi) \geq f_{tr}(w = -\psi)$. This feature of f_{tr} is essential in making a solitary pulse and it manifests itself at the peak of the potential as two counterstreaming beams.

With f_p and f_{tr} , we can now calculate the passing and trapped electron densities separately and obtain

$$n_p = e^\phi \left[1 - \text{erf}(\sqrt{\phi}) \right], \quad (6)$$

$$n_{tr} = \frac{-\phi [1 + 2 \ln(\phi/\psi)]}{\delta^2} + 1 - e^\phi \left[1 - \text{erf}(\sqrt{\phi}) \right]. \quad (7)$$

Note that, even for $\phi \ll 1$, the linearization of n_p gives $n_p \sim 1 - 2\sqrt{\phi/\pi}$ which is different from the leading terms of a Boltzmann distribution. For a Boltzmann distribution, the density $\sim e^\phi$ and the leading terms are $1 + \phi$ (Jackson, 1990). The physical meaning is that under collisionless, self-consistent interaction of electrons and the solitary potential, electrons in the vicinity of the potential are not in local thermal equilibrium, in contrast to the standard starting point of local thermal equilibrium in obtaining the thermal screening length (Debye and Hückel, 1923; Jackson, 1990; Chen, 1984).

To study the contributions from trapped and passing electrons to the charge density ($-\partial^2\phi/\partial x^2$) and how such contributions are affected by various parameters, we show in Fig. 1, plots of n_{tr} and n_p and the charge density ρ as a function of x for several values of ψ and δ . Figures 1a and 1b plot $100 \times n_{tr}(x)$, $100 \times [n_p(x) - 1]$ and $100 \times \rho(x)$ for $(\psi, \delta) = (2 \times 10^{-5}, 0.1)$. For an ambient plasma with $T_e = 700$ eV and $\lambda_D = 100$ m as found at ionospheric heights by the FAST satellite in the environment of BGK EHs (Ergun et al., 1999), this case corresponds to $\psi = 1.4 \times 10^{-2}$ V and $\delta = 10$ m. As shown, in this weakly nonlinear case, the maximum perturbation in n_p is only 0.5% and in n_{tr} 0.4%. The perturbation in the charge density ρ is $\leq 0.2\%$ and occurs within one λ_D . The curves of $n_p(x)$, $n_{tr}(x)$ and $\rho(x)$ for $(\psi, \delta) = (5, 4.4)$ are given in Figs. 1c and d. This choice corresponds to EHs with nearly zero phase space density at the center, $w = -\psi$. That is $f_{tr}(w = -\psi) \sim 0$. One can see that the total charge density perturbation goes $\sim 10\%$ negative and $\sim 25\%$ positive, corresponding respectively to electron density enhancement and depletion. With similar format, Figs. 1e and f plots cases with same δ and $\psi = 1$ to illustrate the change in n_p , n_{tr} and ρ of an EH with equal width but smaller amplitude. The dip in n_{tr} is filled up and the charge density perturbation only increases to 5% positive and 2% negative.

These examples demonstrate how passing electrons produce positive charge density perturbations owing to the decrease in their number density and how the addition of

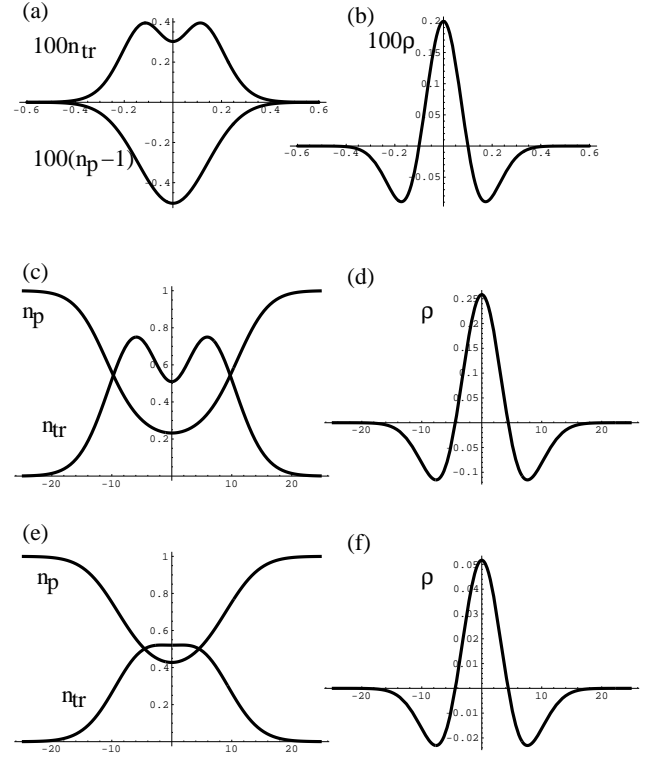


Fig. 1. Trapped electron density (n_{tr}), passing electron density (n_p) and charge density (ρ) for $(\psi, \delta) = (2 \times 10^{-5}, 0.1)$ in (a) and (b), $(\psi, \delta) = (5, 4.4)$ in (c) and (d) and $(\psi, \delta) = (1, 4.4)$ in (e) and (f). These examples illustrate how passing electrons alone would result in the positive charge density perturbation due to their density decrease and how the addition of trapped electrons yields the excess negative charge at the flank.

trapped electrons yields the excess negative charge at the flank. For quantitative illustration, we use a specific potential and an ambient electron distribution but the above result is independent of the specific model that we use and the strength of nonlinearity. To derive that the density of passing electrons must decrease at the positive potential, one only needs the equation of continuity (conservation of charge). Velocities of passing electrons increase at the potential and the density is inversely proportional to the velocity, hence the decrease of their density. Therefore, the excess negative charge cannot be from the passing electrons. It must come exclusively from trapped electrons. In other words, it is the trapped electrons oscillating back and forth inside the solitary potential and carried along by the potential that shield out the positive core of a BGK EH. This unique feature of BGK EHs distinguishes them from positively charged objects dressed in negative thermal charge clouds via Debye shielding mechanism and allows their size to be smaller than λ_D . This feature will be used in the next section as a constraint for the perpendicular boundary condition.

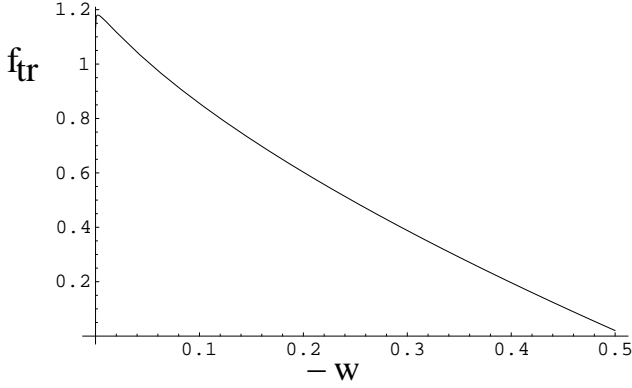


Fig. 2. Trapped electron distribution (Eq. 17) as a function of negative the electron energy ($-w$) for an EH with a perpendicular size $r_s = 5 (\lambda_D)$, parallel width $\delta = 2.1$ and potential amplitude $\psi = 0.5$ at a fixed radial distance. Note that at the center of the phase space EH, $-w = 0.5$, f_{tr} is at its global minimum.

3 Electron holes in 3D magnetized plasma

3.1 The solitary potential

In the following formulation, we will assume azimuthal symmetry, that electron motion is along \mathbf{B} and ions form the uniform background. The first assumption is a natural starting point for a system with a magnetic field. The second is justified since the electron gyroradius (≤ 1 m) is much less than all relevant scale lengths. The third assumption is justified because the velocity perturbation of ions due to the self-consistent interaction with the solitary potential is much smaller than that of electrons owing to the large mass ratio. Therefore, to a good approximation, the ion density can be assumed uniform.

In the wave frame, the 3D Poisson equation and the Vlasov equation for electrons are

$$-\nabla^2 \Phi(\mathbf{r}) = 4\pi\rho(\mathbf{r}), \quad (8)$$

$$\mathbf{v} \cdot \nabla_r F(\mathbf{r}, \mathbf{v}) + \frac{e}{m} \nabla \Phi(\mathbf{r}) \cdot \nabla_v F(\mathbf{r}, \mathbf{v}) = 0, \quad (9)$$

where Φ is the electrostatic potential, ρ the charge density and F the electron distribution function. The second term in the Vlasov equation is the nonlinear term that makes solitary wave solutions possible. Equation (8) written in the cylindrical coordinate system (r, θ, z) with azimuthal symmetry is

$$\left[\frac{\partial}{r \partial r} + \frac{\partial^2}{\partial r^2} + \frac{\partial^2}{\partial z^2} \right] \Phi(r, z) = -4\pi\rho(r, z). \quad (10)$$

Equation (10) has only two variables but it is not a 2D Poisson equation because they differ by the term $\frac{\partial}{r \partial r}$. We search for solutions which give a single humped potential $\Phi(\mathbf{r})$, that is, $\Phi(\mathbf{r})$ has no node. The feature derived in the last section, screening-by-trapped-electrons, only applies in the parallel direction as trapped electrons cannot oscillate perpendicular to the magnetic field. This implies that the charge density

should not change sign in the perpendicular direction and this leads us to the eigenfunction of the differential operator $(\frac{\partial}{r \partial r} + \frac{\partial^2}{\partial r^2})$; the Bessel function zero. The solitary potential constructed according to this boundary condition yields

$$\Phi(\mathbf{r}) = \phi_{\parallel}(z) J_0\left(k_{00} \frac{r}{r_s}\right), \quad (11)$$

where $k_{00} \simeq 2.404$ is the first root of Bessel function J_0 , r_s is the perpendicular scale size at which Φ falls to zero and $\phi_{\parallel}(z)$ the parallel profile of the solitary potential.

J_0 comes into our solution because electrons associated with EHs are highly field-aligned and the same mechanism of screening-by-trapped-electrons of BGK EHs in the parallel direction does not apply in the perpendicular direction. The perpendicular boundary condition set by this physical constraint selects J_0 , the eigenfunction of the radial differential operator. This means that the charge density

$$\rho(r, z) = \frac{J_0(k_{\perp} r) \phi_{\parallel}(z)}{4\pi} \left[k_{\perp}^2 + \frac{1 + 2 \ln(\phi_{\parallel}/\Psi)}{\delta^2} \right], \quad (12)$$

and the potential have exactly the same radial function as their perpendicular profiles. This feature can be experimentally verified if EHs can be measured along the perpendicular direction. One would observe that variations in the charge density and the electrostatic potential track each other with different scaling coefficients.

The structure of the solitary potential, Φ , the corresponding electric field,

$$\begin{aligned} \mathbf{E} &= E_r(r, z) \hat{r} + E_z(r, z) \hat{z} \\ &= \hat{r} \left[-\phi_{\parallel}(z) \frac{\partial J_0(k_{\perp} r)}{\partial r} \right] + \hat{z} \left[J_0(k_{\perp} r) \frac{\partial \phi_{\parallel}(z)}{\partial z} \right], \end{aligned} \quad (13)$$

and the charge density will be illustrated later after we discuss the physical parameter range in which there exist electron distributions to support the potential.

3.2 The trapped electron distribution

We now use the potential as given by Eq. (11) to obtain the trapped electron distribution to demonstrate that the plasma can kinetically support such a potential. With the assumption that electrons only move along \mathbf{B} , Eq. (9) in normalized units becomes

$$v \frac{\partial F(r, z, v)}{\partial z} + \frac{1}{2} \frac{\partial \Phi(r, z)}{\partial z} \frac{\partial F(r, z, v)}{\partial v} = 0. \quad (14)$$

Equation (14) stipulates that, for any $r \leq r_s$, there exists a 1D Vlasov equation in the parallel direction; but these parallel Vlasov equations for different r are not independent. Instead, their mutual relation in the perpendicular direction is determined by the perpendicular profile of Φ . This is because Φ is the potential produced collectively by the plasma particles. Once Φ is known, how the plasma distributes itself to self-consistently support the potential is determined. Therefore, we need only to solve the equation for a particular r . Setting $r = \bar{r}$, a constant, define

$$\begin{aligned} \phi(z) &= \Phi(\bar{r}, z) = J_0(k_{\perp} \bar{r}) \phi_{\parallel}(z), \\ f(z, v) &= F(W(\bar{r}, z, v)), \end{aligned}$$

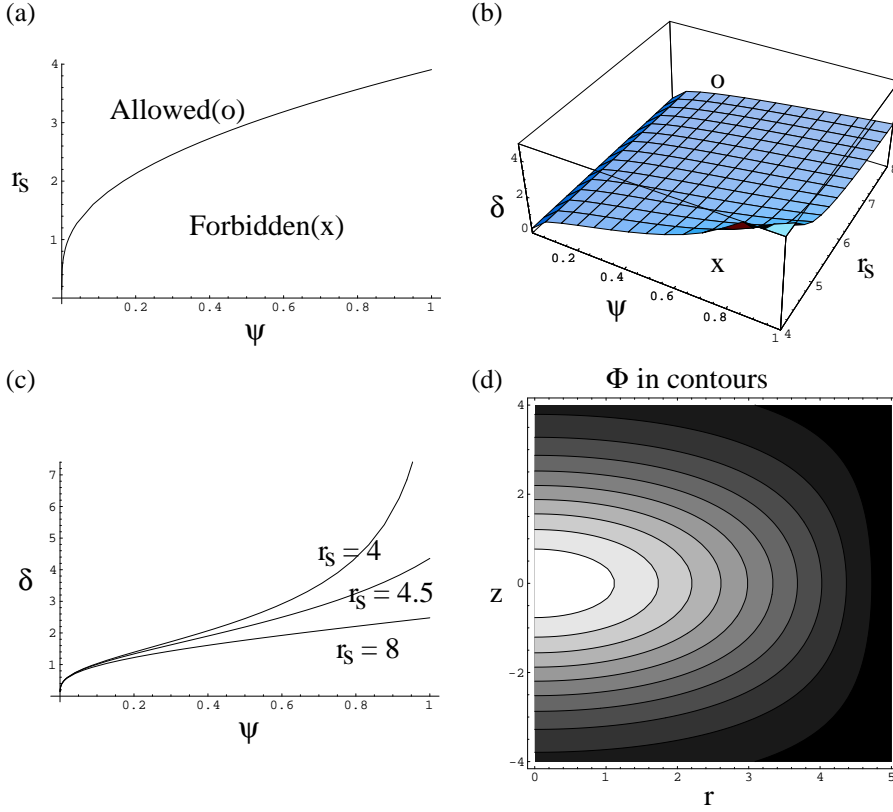


Fig. 3. The inequality relation (Ineq. 19) between the perpendicular size (r_s) and the potential amplitude (ψ): (a) the relation (Ineq. 18) between the perpendicular size, parallel size (δ) and the amplitude, (b) three r_s cuts showing the dependence of the parallel width (δ)-amplitude (ψ) relation on the perpendicular size, (c) a sample solitary potential as a function of z and r , (d). Solitary potentials can take (r_s, δ, ψ) values in regions marked Allowed (O). Regions marked Forbidden (X) give unphysical trapped electron distributions and are thus not allowed.

where $W = v^2 - \Phi(r, z)$ is the total energy of an electron and $F(W)$ is a solution to Eq. (14), as can be readily verified. Now substitute the potential constructed in Eq. (11) into Eq. (10), replace r by \bar{r} and re-write $\rho(\bar{r}, z)$ in terms of the trapped and passing electron distribution, f_{tr} and f_p , respectively. In terms of these variables, Eq. (10) becomes

$$\begin{aligned} \frac{\partial^2 \phi(z)}{\partial z^2} - k_{\perp}^2 \phi(z) &= \int_{-\phi}^0 dw \frac{f_{tr}(w)}{2\sqrt{w+\phi}} \\ &+ \int_0^{\infty} dw \frac{f_p(w)}{2\sqrt{w+\phi}} - 1, \end{aligned} \quad (15)$$

where $k_{\perp} = \frac{k_{00}}{r_s} \simeq \frac{2.404}{r_s}$ and $w = W(\bar{r}, z, v) = v^2 - J_0(k_{\perp} \bar{r}) \phi_{\parallel}(z)$ is the total energy of an electron at \bar{r} travelling along z . Electrons with $w \geq 0$ are untrapped and electrons with $w < 0$ are trapped. Equation (15) differs from its counterpart in the 1D model by the term $k_{\perp}^2 \phi$ which couples the perpendicular part of the solitary wave into its parallel equation. The larger the perpendicular size, r_s , the closer Eq. (15) approaches its counterpart in the 1D model. In the limiting case, when r_s approaches infinity, the solution reduces to the 1D solution which describes infinitely large charge sheets perpendicular to **B** and propagating along **B**. This is exactly the equivalent 3D system of the 1D model. The perpendicular size of the solitary wave determines whether a spacecraft would be able to see the 3D structure or only the parallel feature. This offers a plausible explanation as to why, in the magnetosphere, both multi and one dimensional

solitary waves are seen. (See Ergun et al. (1999) for multi-dimensional cases and Bale et al. (1998) and Matsumoto et al. (1994) for 1D cases.)

To obtain f_{tr} , we follow the BGK approach with Maxwellian ambient electrons,

$$F_p(W) = \frac{2}{\sqrt{\pi}} e^{-W}, \quad (16)$$

For convenience, define $J_0(k_{\perp} \bar{r}) \Psi$ as ψ . The trapped electron distribution obtained from Eq. (15) then reduces to

$$\begin{aligned} f_{tr}(w) &= -\frac{4k_{\perp}^2}{\pi} \sqrt{-w} + \frac{4\sqrt{-w}}{\pi \delta^2} \left[1 - 2 \ln \left(\frac{-4w}{\psi} \right) \right] \\ &+ \frac{2e^{-w}}{\sqrt{\pi}} \left[1 - \text{erf}(\sqrt{-w}) \right]. \end{aligned} \quad (17)$$

Different perpendicular, parallel widths and potential amplitudes give different constants and coefficients to $f_{tr}(w)$ and thus yield different f_{tr} values. Some combinations of (r_s, δ, ψ) can give negative f_{tr} values and this means that there does not exist an electron distribution to support the potentials with these (r_s, δ, ψ) parameters. As an example, we plot f_{tr} as a function of $-w$ in Fig. 2 for a physical combination: (r_s, δ, ψ) = (5, 2.1, 0.5). f_{tr} is positive for the entire range of its argument and its global minimum is at $-w = \psi$, the center of the phase space EH.

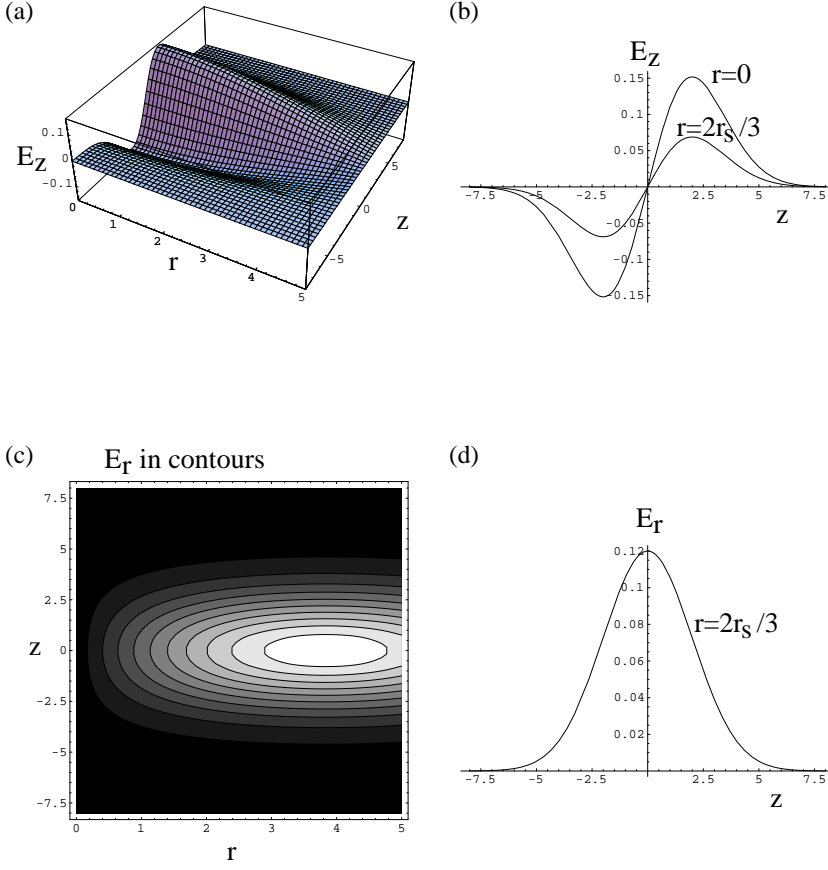


Fig. 4. (a) and (c) The parallel (E_{\parallel}) and perpendicular (E_{\perp}) components of the electric field for the constructed BGK solitary wave, (b) two parallel cuts of E_{\parallel} along the symmetry axis ($r = 0$) and along $r = 2r_s/3$. These are symmetric bipolar pulses. (d) a parallel cut of E_{\perp} along $r = 2r_s/3$. This is unipolar just as observed in space observations.

3.3 Inequality relations between parallel, perpendicular scale sizes and the amplitude

For the solution (Eq. 17) to be physical, $f_{ir}(w)$ has to be non-negative. Since $f_{ir}(0 > w \geq -\psi) \geq f_{ir}(w = -\psi)$, the condition $f_{ir}(w = -\psi) \geq 0$ suffices to satisfy the requirement. From this condition, we obtain an inequality relation between δ , ψ and r_s ,

$$\delta \geq \sqrt{\frac{4 \ln 2 - 1}{\sqrt{\pi} e^{\psi} (1 - \operatorname{erf}(\sqrt{\psi})/2\sqrt{\psi} - 2.404^2/r_s^2)}}. \quad (18)$$

We do not restrict ourselves to empty-centered EHs (EHs with $f_{ir}(w = -\psi) = 0$) and therefore, for an allowed pair of (ψ, r_s) , any δ that satisfies inequality 18 is allowed. In other words, for a fixed amplitude and perpendicular scale size, the parallel scale size has a lower bound but no upper bound. The lower bound corresponds to EHs with no trapped electrons at rest at the bottom of the potential energy troughs; that is, the centers of the phase space structures are empty (hence, called empty-centered EHs). The denominator on the RHS of inequality 18 has to be positive. This yields another inequality relation between ψ and r_s ,

$$r_s > \frac{2.404}{\sqrt{\sqrt{\pi} e^{\psi} (1 - \operatorname{erf}(\sqrt{\psi})/2\sqrt{\psi})}}. \quad (19)$$

Ineq. (19) means that, for a given potential amplitude, the perpendicular scale size of EHs is greater than a critical value

given by the RHS as a function of the potential amplitude in order to have a physical electron distribution to support the solitary potential.

Figures 3a–c show plots of the allowed parameter range with Fig. 3a representing Ineq. (19), Fig. 3b Ineq. (18) and Fig. 3c r_s cuts of Ineq. (18). For a solitary potential Φ with a peak amplitude Ψ , the perpendicular size r_s has to satisfy Ineq. (19) with the ψ on the RHS replaced by Ψ . For example, if Ψ is 0.5 (in units of T_e/e), the perpendicular size is roughly greater than 3 (in units of λ_D). We indicate the allowed region by O and the forbidden by X in Figs. 3a and b. Any (δ, Ψ, r_s) lying on or above the shaded surface is allowed. For example, for $\Psi = 100$ (corresponding to 10 kV for $T_e = 100$ eV) and $r_s = 100$ (corresponding to 10 km for $\lambda_D = 100$ m) the parallel scale size δ can be as small as 20 (λ_D) and as large as several earth radii (R_E) or even larger. We can look at another example with $\Psi = 10^{-4}$ (corresponding to 10 mV for $T_e = 100$ eV) and $r_s = 0.2$ (corresponding to 20 m for $\lambda_D = 100$ m), when δ is at least 0.12 (λ_D) or larger. The inequality nature of the width-amplitude-perpendicular size relation means that the plasma permits BGK EHs with any parallel width ranging from less than 1 λ_D to greater than 1 R_E . Figure 3c shows the dependence of the parallel width-amplitude ($\delta - \psi$) relation on the perpendicular size r_s . With a fixed r_s , the empty-centered EHs (corresponding to the equal sign in Ineq. 18) give the largest

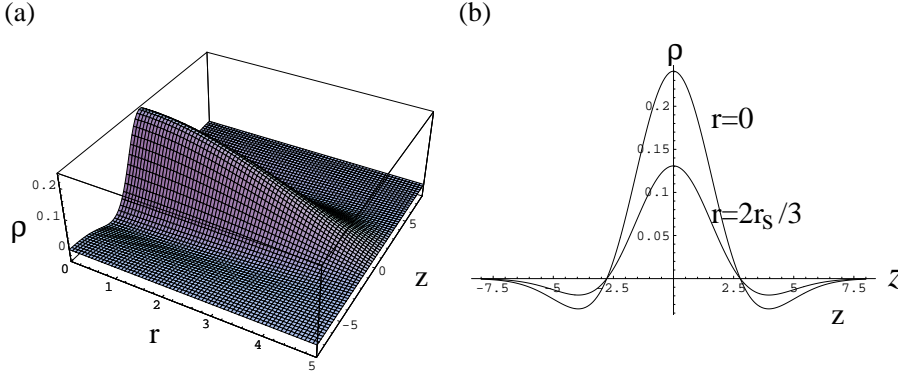


Fig. 5. (a) the charge density for the constructed BGK solitary wave. (b) two parallel cuts of the charge density along the symmetry axis ($r = 0$) of the solitary wave and along $r = 2r_s/3$. The excursions along the symmetry axis are the largest, comparing to other parallel cuts of the charge density.

amplitudes for the same δ . For the same amplitude, EHs with larger r_s have smaller lower bounds for δ . This dependence of the parallel width-amplitude relation on the perpendicular size can be used in conjunction with the measured width-amplitude scatter plot to give an estimate of the typical perpendicular size of EHs. For example, if the measured parallel widths and amplitudes (unbinned) lie between the lines for $r_s = 4$ and $r_s = 8$, we know that the typical perpendicular size for these EHs is $4-8 \lambda_D$. We can then estimate how much electrostatic energy is transported by each of these EHs by multiplying the measured energy density (square of the electric field amplitude), the parallel width and the cross sectional area with the above radius.

3.4 The structure of the potential, electric field and charge density

We next examine the structure of the potential and comparisons this within observations. As the solitary waves travel along \mathbf{B} with typical velocity ~ 1000 km/s and pass the spacecraft, the measurement taken on the spacecraft is analogous to taking parallel cuts of the involved quantities. We will plot the parallel cuts for comparison with the observations.

Figure 3d plots an example of the solitary potential Ψ as a function of r and z with $r_s = 5$, $\Psi = 0.5$, and $\delta = 2.1$, in the allowed parameter range. Positive z is along the direction of the magnetic field. The potential peaks at the center and monotonically drops to zero in the parallel direction as a Gaussian and perpendicularly as a Bessel zero. The electric field of the solitary structure vanishes at the center and points outward away from the center. The parallel component of the electric field, $E_z \equiv E_{\parallel}$, is shown in Fig. 4a as a function of r and z . Two parallel cuts of E_{\parallel} at $r = 0$ and $r = r_s/1.5$ are shown in Fig. 4b. For any $\bar{r} < r_z$, $E_{\parallel}(\bar{r}, z)$ is symmetric and bipolar. On the symmetry axis, $r = 0$, the maximum excursion of E_{\parallel} is the largest and, as r increases, it falls off as $J_0(k_{\perp}r)$. The perpendicular component of the electric field, $E_r \equiv E_{\perp}$, is plotted in Fig. 4c as a contour plot to aid in the visualization of its parallel cuts. One example of the parallel cuts is shown in Fig. 4d and it is unipolar. Any parallel cut of E_{\perp} is unipolar except the one along the sym-

metry axis ($r = 0$) where E_{\perp} is zero. Note that E_{\perp} is not zero at the perpendicular boundary, $r = r_s$, so perpendicular screening from the ambient electrons is needed to facilitate the decrease of E_{\perp} to zero. This perpendicular screening is not described by our solution.

The charge distribution, ρ , as a function of r and z is presented in Fig. 5a, and two parallel cuts of ρ are depicted in Fig. 5b. Note that, as the radial distance from the symmetry axis increases, the measured charge density perturbation becomes smaller. Along the symmetry axis, the charge density variation is the largest with the positive excursion reaching $\sim 24\%$ and the negative $\sim 4\%$. An off-centered cut along $r = r_s/1.5$ with a positive excursion $\sim 13\%$ and $\sim 2\%$ negative is also shown.

4 Summary and conclusion

We have obtained new results for 1D BGK electron solitary waves and, based on the 1D results, we have extended the solutions incorporating the 3D electric interaction of the plasma. One key feature of a 1D BGK EH is that its positive core is shielded by electrons trapped and oscillating inside the solitary potential. Since the thermal screening from the ambient plasma is not needed, the size of a 1D BGK EH can be smaller than one λ_D (an example can be found in Figs. 1a and b). The 3D solution preserves the properties of 1D solutions in the direction parallel to the magnetic field, hence it is like a perpendicularly confined bundle of 1D BGK EHs. In 3D BGK EHs, as electrons are highly field-aligned, trapped electrons can oscillate back and forth along the direction of the magnetic field and, as a consequence, the screening-by-trapped-electrons in 1D still applies in the parallel direction. Since thermal screening is not needed in the parallel direction, the parallel widths of the 3D BGK EHs can also be smaller than one λ_D . We therefore predict that multi-dimensional BGK EHs in magnetized plasma can have parallel widths smaller than the Debye scale.

The extension to three dimensions utilizes the key feature, screening by trapped electrons, of 1D BGK EHs. This feature is an essential part of the boundary condition from which we obtain Bessel function zero, J_0 , for the perpendic-

ular profiles of the potential and charge density. The observable is that the perpendicular cuts of the solitary potential and charge density would track each other with different scaling coefficients.

We derived the physical parameter range within which the plasma can self-consistently support the solitary potential. The relations between the parallel and perpendicular scale sizes and the potential amplitude are inequalities. The inequality relations permit EHs of large scales with reasonable potential amplitudes. The inequality relation between the three parameters indicates a dependence on the perpendicular size of the parallel width and amplitude relation. This dependence can be used in conjunction with experimental data to give an estimate of the typical perpendicular size of EHs. This information is a measure of the perpendicular span of the EH source region and provides an estimate of the amount of electrostatic energy transported by the solitary waves.

Finally, note that this paper has analytically modeled the electric field bipolar pulses as BGK electron holes that are time stationary solutions of the nonlinear Vlasov-Poisson equations. We have not addressed the problem associated with the dynamical and evolutionary features of the EHs that have been addressed by numerical simulations (Oppenheim et al., 1999; Singh et al. 2000; Muschietti et al. 2000; Newman et al. 2001).

Acknowledgements. The research at the University of Washington and the Space Sciences Laboratory at Berkeley is supported in part by NASA grants NAG5-3170 and NAG5-26580.

References

- Bale, S. D., Kellogg, P. J., Larson, D. E., Lin, R. P., Goetz, K., and Lepping, R. P.: Bipolar electrostatic structures in the shock transition region: Evidence of electron phase space holes, *Geophys. Res. Lett.*, 25, 2929–2932, 1998.
- Berk, H. L., Nielsen, C. N., and Roberts, K. V.: Phase space hydrodynamics of equivalent nonlinear systems: experimental and computational observations, *Phys. Fluids*, 13, 980–995, 1970.
- Bohm, D. and Gross, E. P.: Theory of plasma oscillations, *Phys. Rev.*, 75, 1851–1864, 1949.
- Bernstein, I. B., Greene, J. M., and Kruskal, M. D.: Exact nonlinear plasma oscillations, *Phys. Rev.*, 108, 546–550, 1957.
- Boström, R., Gustafsson, G., Holback, B., et al.: Characteristics of solitary waves and double layers in the magnetospheric plasma, *Phys. Rev. Lett.*, 61, 82–85, 1988.
- Cattell, C. A., Dombeck, J., Wygant, J. R., et al.: Comparisons of Polar satellite observations of solitary wave velocities in the plasma sheet boundary and the high altitude cusp to those in the auroral zone, *Geophys. Res. Lett.*, 26, 425–428, 1999.
- Chen, F. F.: Introduction to plasma physics and controlled fusion, Plenum Press, 1984.
- Davidson, R. C.: Methods in nonlinear plasma theory, Academic Press, 1972.
- Davydov, A. S.: Solitons in Molecule Systems, McGraw-Hill, 1985.
- Debye, P. and Hückel, E.: Zur theorie der elektrolyte, *Physik. Zeits.*, 24, 185, 1923.
- Drazin, P. G.: Solitons, Cambridge University Press, 1984.
- Ergun, R. E., Carlson, C. W., McFadden, J. P., et al.: FAST satellite observations of large-amplitude solitary structures, *Geophys. Res. Lett.*, 25, 2041–2044, 1998.
- Ergun, R. E., Carlson, C. W., McFadden, J. P., Mozer, F. S., Muschietti, L., and Roth, I.: Debye-scale plasma structures associated with magnetic-field-aligned electric fields, *Phys. Rev. Lett.*, 81, 826–829, 1998.
- Ergun, R. E., Carlson, C. W., Muschietti, L., Roth, I., and McFadden, J. P.: Properties of fast solitary structures, *Nonlinear Processes in Geophysics*, 6, 187–194, 1999.
- Eriksson, A. I., Mälkki, A., Dovner, P. O., Boström, R., Holmgren, G., and Bolback, B.: A statistical survey of auroral solitary waves and weak double layers 2. Measurement accuracy and ambient plasma density, *J. Geophys. Res.*, 102, 11 385–11 398, 1997.
- Franz, J., Kintner, P. M., and Pickett, J. S.: POLAR observations of coherent electric field structures, *Geophys. Res. Lett.*, 25, 1277–1280, 1998.
- Goldman, M. V., Oppenheim, M. M., and Newman, D. L.: Theory of localized bipolar wave-structures and nonthermal particle distributions in the auroral ionosphere, *Nonlinear Processes in Geophysics*, 6, 221–228, 1999.
- Hasegawa, A. and Kodama, Y.: Solitons in Optical Communications, Clarendon Press, 1995.
- Jackson, J. D.: Classical Electrodynamics, John Wiley & Sons, 1990.
- Kojima, H., Matsumoto, H., Chikuba, S., Horiyama, S., Ashour-Abdalla, M., and Andersson, R. R.: Geotail wave form observations of broadband/narrowband electrostatic noise in the distant tail, *J. Geophys. Res.*, 102, 14 439–14 455, 1997.
- Krall, N. A. and Trivelpiece, A. W.: Principles of Plasma Physics, McGraw-Hill, 1973.
- Krasovsky, V. L., Matsumoto, H., Omura, Y., et al.: Interaction dynamics of electrostatic solitary waves, *Nonlinear Processes in Geophysics*, 6, 205–209, 1999.
- Matsumoto, H., Kojima, H., Mijatake, T., Omura, Y., Okada, M., Nagano, I., and Tsutsui, M.: Electrostatic solitary waves (ESW) in the magnetotail: BEN wave forms observed by Geotail, *Geophys. Res. Lett.*, 21, 2915–2918, 1994.
- Matsumoto, H., Kojima, H., Omura, Y., and Nagano, I.: Plasma waves in geospace: GEOTAIL observations, *New Perspective on the Earth's Magnetotail*, *Geophys. Monog.*, 105, 259–319, 1998.
- Mozer, F. S., Ergun, R. E., Temerin, M., Cattell, C., Dombeck, J., and Wygant, J.: New features of time domain electric-field structures in the auroral acceleration region, *Phys. Rev. Lett.*, 79, 1281–1284, 1997.
- Muschietti, L., Ergun, R. E., Roth, I., and Carlson, C. W.: Phase-space electron holes along magnetic field lines, *Geophys. Res. Lett.*, 26, 1093–1096, 1999.
- Muschietti, L., et al.: Transverse instability of magnetized electron holes, *Phys. Rev. Lett.*, 85, 94–97, 2000.
- Mälkki, A., Koskinen, H., Boström, R., and Holback, B.: On theories attempting to explain observations of solitary waves and weak double layers in the auroral magnetosphere, *Phys. Scr.*, 39, 787–793, 1989.
- Mälkki, A., Eriksson, A. I., Dovner, P. O., et al.: A statistical survey of auroral solitary waves and weak double layers 1. Occurrence and net voltage, *J. Geophys. Res.*, 98, 15 521–15 530, 1993.
- Newman, D. L., Goldman, M. V., Spector, M., and Perez, F.: Dynamics and instability of electron phase-space tubes, *Phys. Rev. Lett.*, 86, 1239–1242, 2001.
- Oppenheim, M. M., Newman, D. L., and Goldman, M. V.: Evolution of electron phase-space holes in 2-D magnetized plasma, *Phys.*

- Rev. Lett., 73, 2344–2347, 1999.
- Roberts, K. V. and Berk, H. L.: Nonlinear evolution of a two-stream instability, Phys. Rev. Lett., 19, 297–300, 1967.
- Schamel, H.: Electron holes, ion holes and double layers, Phys. Rep., 140, 161–191, 1986.
- Singh, N., Loo, S. M., Wells, B. E., and Daverapalli, C.: Three-dimensional structure of electron holes driven by an electron beam, Geophys. Res. Lett., 27, 2469–2472, 2000.
- Temerin, M., Cerny, K., Lotko, W., and Mozer, F. S.: Observations of double layers and solitary waves in the auroral plasma, Phys. Rev. Lett., 48, 1175–1178, 1982.
- Turikov, V. A.: Electron phase-space holes as localized BGK solutions, Phys. Scr., 30, 73–77, 1984.